TOPEX Microwave Radiometer Performance Evaluation, 1992–1998

Stephen J. Keihm, Victor Zlotnicki, *Member, IEEE,* and Christopher S. Ruf, *Senior Member, IEEE*

***Abstract*—The stability and accuracy of the TOPEX Microwave Radiometer (TMR) measurement of the atmospheric path delay due to water vapor is assessed over the interval from launch (August 1992) through June 1998. Detailed global comparisons are made with path delays derived from the special sensor microwave imager (SSM/I) instruments and a network of 15 island radiosondes. The results provide consistent evidence that the TMR path delay measurements included an instrument-related downward drift of 1.0–1.5 mm/yr between October 1992 and December of 1996. The four-year drift correlates with an upward drift seen in the coldest TMR 18-GHz brightness temperature time series and is further supported by independent comparisons of TMR with ERS-1 and 2, GPS, and the Harvest Platform water vapor radiometer measurements. From January 1997 through June 1998, no significant relative path delay drift between TMR and SSM/I is seen in the comparison data, although anomalies do appear in early 1998. In terms of accuracy, both the SSM/I and radiosonde comparisons indicate no significant ($>2\%$) scale error in the TMR path delay. An overall bias of <10 mm may be present, but the comparisons are not consistent in this determination.**

***Index Terms*—Microwave radio propagation, microwave radiometry, meteorological factors, path delay, radiosondes, remote sensing.**

I. Introduction

SINCE its launch in August 1992, the TOPEX/Poseidon (T/P) satellite mission has established new standards for the accuracy and precision of altimetric measurements of sea surface height. The original mission requirements [1] for the T/P system called for a root-sum-squared error in a 1-s sample of sea surface height above the ellipsoid of 137 mm. Shortly after launch, the error was assessed to be 47 mm [2] and today, the value is believed to be closer to 43 mm (Fu, 1999, pers. comm.). However, with appropriate space-time filtering, investigators have retrieved much smaller signals, utilizing knowledge of the signal's space-time correlation and propogation characteristics. For example, Le Provost and coworkers [3] recovered the major tidal constituents from T/P and a numerical model of 28 mm. Chambers and coworkers [4] related seasonal sea level changes to oceanic heat storage rates, detecting signals of order 1 W/m^2 (equivalent to $\sim$2 mm of sea level variation) when averaged over entire ocean basins. Minster and co-workers [5] detected seasonal changes in globally-averaged mean sea levels with 9.5 mm amplitude, which they related to the global water cycle.

A critical supporting measurement for the sea level determinations is provided by the TOPEX microwave radiometer (TMR), a three-channel, nadir-viewing instrument that measures the water vapor-induced delay in the radar path [6]–[8]. In terms of path length, the vapor-induced delay produces 40–900 mm additional path delay, highly variable in time and space, for the two-way altimeter signal. The mission requirement for TMR performance, 12 mm root mean square (rms) accuracy [1], appeared to be satisfied following algorithm tuning implemented after the first six months' cal/val phase [9]. However, with over six years of operation now completed, much more extensive evaluation of the TMR performance can be made, including comparisons with other satellite radiometers [10] and analysis of long term instrument drifts [11], [12]. These evaluations have become meaningful at the level of millimeters, as the demonstrated altimetric precision has approached or surpassed the centimeter level in both the spatial and temporal domains. For example, the predicted response of the ocean to greenhouse warming is a global sea level rise of $\sim$3–6 mm/yr [13], and investigators have attempted to extract trends of even smaller magnitude from the TOPEX data [14]. Potential altimeter and radiometer instrument drifts must be carefully monitored at these levels in order to extract the correct geophysical trends. Mitchum [15] showed that comparisons of the TOPEX sea level measurements with the global tide gauge network indicated a relative drift of $\sim$2 mm/yr (TOPEX decreasing) over the 1992–1997 interval, a signal comparable in magnitude to the effect predicted by greenhouse warming. Because the trend exhibited a latitude dependence (higher trends in wet, tropical regions), a downward fractional drift in the TMR path delay correction was considered as a possible explanation.

The Mitchum tide gauge results, well known within the satellite altimetry community prior to its 1998 publication [15], provided the primary motivation for the recent attempts to assess possible TMR path delay drifts of order 1 mm/yr. These studies, described briefly in Section III, yield fairly consistent results in terms of TMR drifts relative to independent measurements of the vapor-induced path delay. However, the results may be questioned due to sparseness and site-specific limitations of the ground-based independent measurements and calibration drift uncertainties of the comparison satellite radiometers. We therefore sought large comparison data sets with global representation and demonstrated calibration stability to both better constrain possible drifts in the TMR path delay measurements and assess the overall accuracy of the measurements over the first six years of operation.

Manuscript received June 22, 1998; revised December 9, 1999.

S. J. Keihm and V. Zlotnicki are with the Jet Propulsion Laboratory, California Institute of Technology, Pasadena, CA 91109 USA (e-mail: stephen.j.keihm@jpl.nasa.gov).

C. S. Ruf is with The Pennsylvania State University, University Park, PA 16802 USA.

Publisher Item Identifier S 0196-2892(00)04128-0.

The first global comparison data set selected derives from the series of special sensor microwave imager (SSM/I) instruments flown by the Defense Meteorological Satellite Program (DMSP) [16]. The SSM/I instrument consists of a seven-channel, four-frequency radiometer operating at 19.3, 22.2, 37.0, and 85.5 GHz. All channels receive both vertically and horizontally polarized radiation at an earth-incidence angle of 53.41°, with the exception of the 22.2 GHz channel, which receives vertical only. The conical scan geometry produces nearly complete global coverage over 24-h intervals.

An initial concern with SSM/I-TMR global comparisons was a possible diurnal effect due to the differences in the SSM/I and TMR orbits. The SSM/I orbits are sun-synchronous (near constant ascending and descending ground track local times), while the TMR ground track local time is uniformily distributed over the entire day. Thus, SSM/I and TMR averages might be expected to differ due to persistent diurnal patterns. To evaluate this effect, we examined the dependence of TMR-derived path delays on local time for narrow latitude bins using the first three years of data. We found no significant diurnal signal in the results, with typical peak-to-peak scatter of less than 3% in path delay, indicating that global comparisons of over-ocean water vapor abundances are not biased by diurnal effects.

Geophysical data products derived from the Wentz ([17], [18]) algorithms were obtained from the Remote Sensing Systems web site. The water vapor-related data product is the precipitable water vapor column, which is closely related to path delay (see Section II). Intercalibration of the four SSM/I instruments (DMSP satellites F08, F10, F11, and F13) included in the study was done in the antenna temperature domain using collocated data obtained when the two most recent instruments were both operational, resulting in an estimated intercalibration accuracy of 0.1 K [17]. It is our view that the ocean coverage, number of channels, and demonstrated quality of the geophysical algorithms make the SSM/I data an excellent comparison set for the six year TMR evaluation.

The second selected comparison data set consists of a global network of 15 island radiosonde stations that lie within 300 km of the TOPEX groundtrack. Data from these stations were used to establish the final production mode algorithms for TMR following the cal/val phase [9]. The continuous accumulation of radiosonde data from these sites provides a critical ground reference archive for TMR evaluation, which does not depend on radiometric calibration.

This paper is organized as follows. In Section II, the methodology for comparing SSM/I and radiosonde data with TMR measurements in the path delay domain is described. In Section III, the TMR drift relative to SSM/I is evaluated over the 1992–1998 time frame, including dependencies of the drift on latitude and path delay level. Section III also includes TMR drift results derived by other investigators using ground-based and satellite data. In Section IV, we describe an analysis of long-term TMR brightness temperature time series data, which separates instrument-related drifts from atmospheric effects. The results are examined in terms of their consistency with the TMR path delay drifts inferred from the comparison data. In Section V, we present constraints on TMR path delay offset and scale errors provided by the SSM/I and radiosonde comparisons. A summary discussion is presented in Section VI, including comments on the limitations of the comparison analyses.

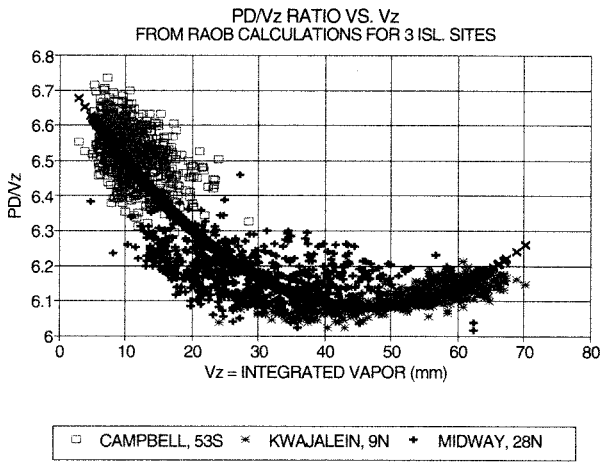

Fig. 1. Relationship between columnar vapor Vz and zenith wet path delay PD derived from radiosonde computations.

II. SSM/I and Radiosondes versus TMR: Comparison Methodology

With nearly complete global coverage every 24 h, the SSM/I data provide an excellent source for comparisons with TMR path delay measurements. In the present study, we used the SSM/I data processed by Wentz [17], [18]. The SSM/I data product most closely related to path delay is integrated vapor, and a conversion is required from integrated vapor to radar path delay that accounts for the $1/T$ (T = Kelvin temperature) dependence of the vapor-induced refractivity. The conversion utilizes the correlation between high vapor content and high tropospheric temperatures estimated from island radiosondes. From each radiosonde profile of temperature and humidity, both integrated vapor Vz and path delay PD are computed as in [8], using the Boudouris [19] formulation for the vapor-induced refractivity. Fig. 1 shows a scatterplot of the ratio PD/Vz against Vz computed from three island radiosonde data archives, which represent dry, moderate, and high humidity conditions. A fit to the data provides the conversion algorithm that was applied to the SSM/I Vz data:

$$PD = 6.759 * Vz - 0.0291 * Vz^2 + 0.000\,31 * Vz^3. \quad (1)$$

In (1), both PD and Vz are measured in mm, and the formal fit error is 2.0 mm. Uncertainties in (1) conversion are important when determining relative offsets and scale errors between SSM/I and TMR (see Section V) but have no significant effect on inferred time trends of the SSM/I-TMR path delay differences.

For the results to be presented, both SSM/I and TMR path delays were averaged over the same 30 day, 1° latitude × 1° longitude bins, then differenced at those bins that contained both SSM/I and TMR data. The SSM/I bins included data from all satellites operating at the specified time (F10, F11 for August 1992 through April 1995; F10, F11, F13 for May 1995 through April 1997; F11, F13, F14 for May 1997 through June 1998). With nearly complete areal coverage over 24 h, the conical scan-

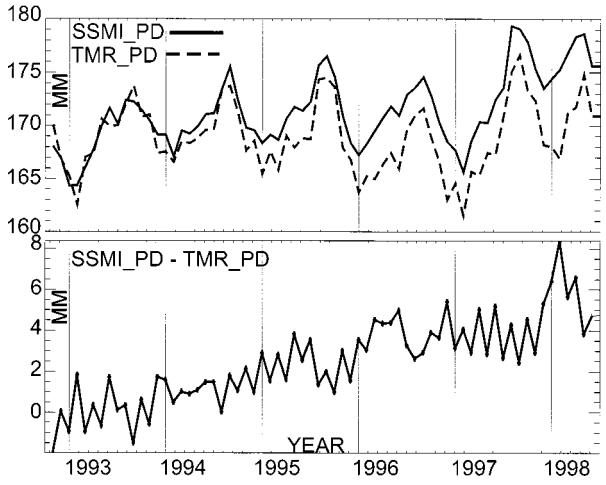

Fig. 2. Time history comparison between TMR- and SSM/I-derived global path delay averages. Each point represents a 30 day averaging over all 1° latitude × 1° longitude bins, which contain both SSM/I and TMR data. Upper panel shows absolute values for both instruments. Lower panel shows the difference time history.

ning SSM/I instruments produce many hundreds of individual measurements in each bin. The nadir viewing TMR, with ∼300 km groundtrack separation at the equator and a ∼10 day repeat orbit, produces fewer than 50 individual measurements for covered bins. However, the adopted approach produces ∼20 000 comparison points per month with global representation sufficient to average down the large temporal decorrelation errors associated with each comparison point and clearly identify relative trends in path delay of order 1 mm/yr.

The radiosonde comparison data were obtained from 15 small island sites lying within 300 km of the TOPEX groundtrack. The radiosonde site locations and groundtrack separations can be found in [9]. Only data within 6 h of radiosonde launch at the times of closest approach were included. The 300 km and 6 h limits on the spatial and temporal separation were chosen as a compromise between the desire to limit decorrelation errors and still produce a sufficiently large sample for statistical reliability. This resulted in ∼3100 comparison points over the 1992–1998 interval.

III. Time "Drift" in TMR Path Delay

Time histories of the 30 day global averages of binned SSM/I and TMR path delay data are shown in Fig. 2 for the period October 1992, shortly after TOPEX launch, to June 1998. Each point in the plots represents the weighted average (by cosine latitude) of all 1° × 1° bins, which included both SSM/I and TMR data over the 30-day interval. In terms of absolute measurement, the agreement between SSM/I and TMR global averages is exceptionally close (within ∼5 mm, upper panel) with comparable seasonal variations but with differences that clearly increase with time and have no apparent seasonality. The early agreement may partially result from the use of Amazon rain forest SSM/I data in the TMR cal/val phase [9]. However, the data was used only to calibrate the TMR high end (over land) brightness temperatures, and no cal/val phase comparisons with over-ocean SSM/I data were made, either in the brightness temperature or path delay domains. Thus, the absolute comparisons remain meaningful.

The SSM/I-TMR difference trend (Fig. 2, lower panel) shows three distinct regimes. Between 10/92 and 12/96 there is a well-defined trend with a fitted slope of 1.4 (±0.2) mm/yr (TMR decreasing relative to SSM/I). Near the beginning of 1997, the difference trend appears to stop until ∼11/97, when a ∼2–4 mm jump occurs. The curve recovers between 6/98 and 6/99 (not shown), suggesting that the late 1997 jump may be related to an aspect of the El Niño event, which impacted the SSM/I and TMR measurement statistics somewhat differently. Additional data will be required to evaluate the late 1998 and later trends. However, as will be shown in Section IV, the SSM/I-TMR behavior between October 1992 and October 1997 correlates closely with a derived instrument-related drift in the TMR 18-GHz channel.

Fig. 2 characterizes the global SSMI-TMR path delay differences. We also binned the SSM/I-TMR data by both latitude and path delay level to look for regional dependencies comparable to those seen in the Mitchum [15] TOPEX-tide gauge sea level difference study. Mitchum found trends in the tropics ($|\text{lat}| < 15^\circ$) ∼ three times greater than the trends in the extratropical ($|\text{lat}| > 15^\circ$) regions. Fig. 3 shows the SSMI-TMR monthly-averaged time series through 1996 for global, tropics, and extratropical subsets. The fitted curves include both annual and linear components, and the results show no significant difference in the trends from the three regions. When the SSM/I-TMR difference is binned by TMR path delay level (Fig. 4), we also see no statistically significant variation in the computed trends. Based on the SSM/I comparisons, we conclude that there is no evidence to support a significant dependence of the TMR time drift on either latitude or path delay level.

As a comparison between two satellite radiometers, subject to many of the same potential errors, the measured SSM/I-TMR relative drift could be attributed to instrument drift in either or both of the radiometers. Other comparisons with either the SSM/I or TMR path delays (or both) are required to properly interpret the SSM/I-TMR results. One such comparison is provided by the radiosonde data base described in Section II. Analysis of the data through December 1996 reveals a relative trend of 1.3 (± 1.0) mm/yr (TMR-radiosonde decreasing), consistent with that found in SSM/I-TMR, but with much larger uncertainty. The main contributors to the uncertainty are the temporal and spatial decorrelation in the 300 km, 6 h window and the sparseness of the data set (relative to SSM/I-TMR). To minimize these effects, the radiosonde-TMR differences were computed as 90 day running averages. However, even after such smoothing, systematic seasonal fluctuations remained (only two of the radiosonde sites are in the Southern Hemisphere), which limited the accuracy of the radiosonde-TMR trend estimate to ∼ ±1.0 mm/yr.

Other investigators have compared the TMR path delay time behavior to the radiometers aboard ERS-1 and ERS-2 ([10]; Urban *et al.*, 1998, pers. comm.) to GPS data [11] and to a ground-based water vapor radiometer at the Harvest oil platform [12], and they have found results consistent with our derived SSM/I-TMR trend for the 1992–1996 time period. These

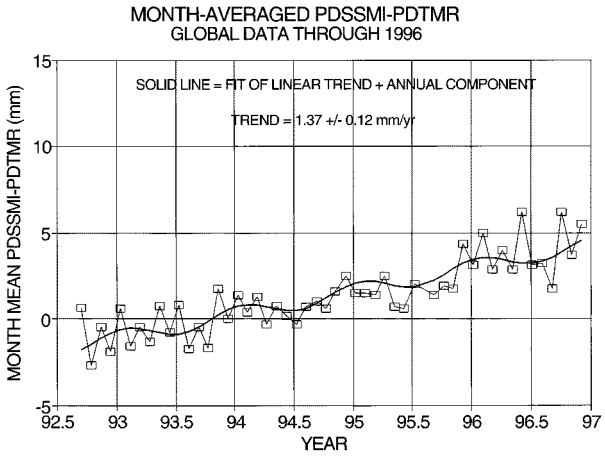

(a)

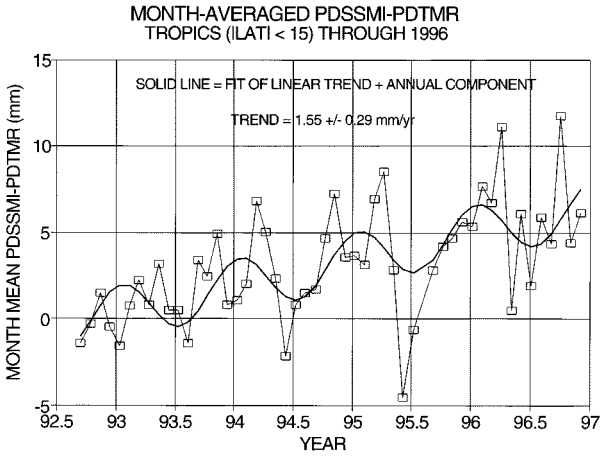

(b)

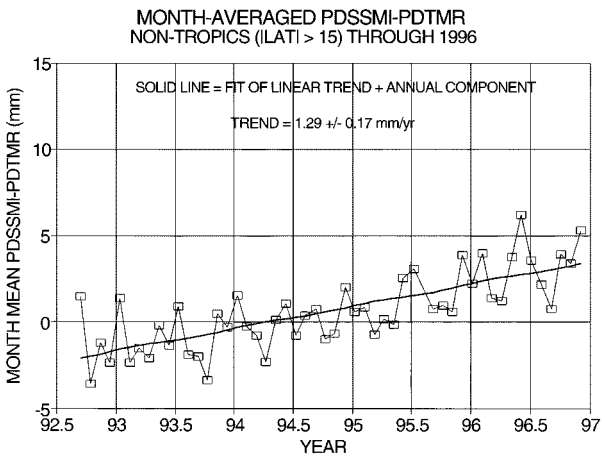

(c)

Fig. 3. SSM/I-TMR path delay differences through 1996 derived using 30 day averages for (a) global, (b) tropics, and (c) extra-tropics data sets.

results are summarized in Table I, along with the trend findings from the present study.

The Harvest Platform WVR comparisons with TMR path delay were coincident in time (to within a few seconds) and closely collocated spatially (∼30 km separation). However, the data base was limited to one comparison point per cycle, and the sparseness of the data accounts for the large statistical uncertainty of the trend fit.

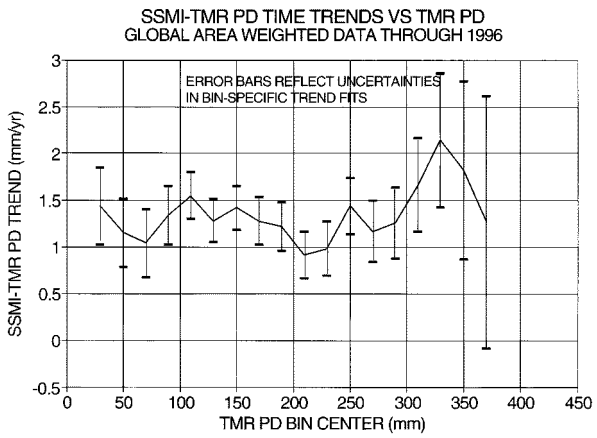

Fig. 4. Linear fit trends of SSM/I-TMR path delay differences determined for 20 mm bins of TMR path delay values.

TABLE I
TMR PATH DELAY TIME DRIFT COMPARISONS

DATA BASE	TIME PERIOD	TREND (mm/yr)	AUTHOR
TMR – WVR at Harvest	11/92 - 12/96	-1.9 +/- 1.2	Kubitschek et al. [12]
TMR – GPS	10/92 – 8/97	-1.2 +/- 0.4	Haines and Bar-Sever, [11]
TMR – ERS-1,2	10/92 - 10/96	-1.3 +/- 0.3	Stum [10], + pers. comm., 1998)
TMR – ERS-1,2	1/93 – 6/96	-1.6 +/- 0.1	Urban et al., pers. Comm., 1998
TMR – ERS-1,2	6/95 – 12/97	-0.8 +/- 0.4	Urban et al., pers. ., Comm., 1998
TMR – Radiosondes	10/92 – 12/96	-1.3 +/- 1.0	(this study)
TMR – SSM/I	10/92 – 12/96	-1.4 +/- 0.2	(this study)

The GPS comparison was also limited to a small set (four stations) spanning the period from late l992 to late 1997. The adopted best estimate drift of -1.2 ± 0.4 mm/yr was based on only two GPS stations (Metsahovi and Onsala) with 45–70 km groundtrack separation and 375 comparison points.

The TMR-ERS result of Stum, -1.3 ± 0.3 mm/yr, is based on ∼four years of comparisons with TMR at ∼14 000 crossover points with less than 1 h time difference, and represents an updated value from an earlier three year study [10]. The results of Urban and coworkers are consistent with both the Stum results and the cessation of the drift early in 1997.

In summary, a drift of -1.3 to -1.4 mm/yr in the TMR-derived path delay over the 10/92–12/96 interval is supported by a wealth of independent data sets and studies. Wentz's claim [17] of 0.1 K intercalibration accuracy in SSM/I antenna temperatures is supported by the absence of discernible discontinuities in the SSM/I-TMR difference and the corroboration of the other TMR comparison studies. The cessation of the TMR drift by early 1997, indicated by the SSM/I-TMR results of Fig. 2, is

supported by direct evidence from an analysis of the time variation of the TMR cold reference brightness temperature statistics, as described in the following section.

IV. TMR Tb Drifts: Separation of Instrumental and Atmospheric Effects

To assess the instrumental cause of the TMR path delay drift, we selected a subset of the brightness temperature data that included only measurements within 10 K of the theoretical over-ocean minimum for each channel. This "cold" data subset, which excludes cloudy and high wind conditions and restricts the analysis to extremely dry conditions, is expected to be least affected by possible long term trends in either atmospheric or ocean surface parameters. In the analysis, a cold reference temperature is calculated for each TMR channel and cycle by extrapolating the cumulative distribution histograms of the cold subsets to the 0% occurrence value. This approach effectively removes any residual component of atmosphere-related or ocean-related variability, and any measurable time trends in the computed cold reference temperature should be indicative of drifts in the instrument. The methodology, described in detail by Ruf [20], is useful for cross-calibrating different satellite radiometers as well as for monitoring individual instruments' calibration drift.

For our purposes, we computed 30-day running averages of the TMR cold reference brightness temperatures between October 1992 and June 1998 (Fig. 5). In the 18-GHz channel [Fig. 5(a)], a clear upward trend (0.27 K/yr by linear regression) is seen in the time series, beginning at launch and ending in the December 1996–January 1997 time frame. This feature strongly correlates with the SSM/I-TMR path delay difference seen in Fig. 2(b), further confirming that the relative drift is attributable to a TMR instrument drift. The fact that no statistically significant drift can be seen in the TMR 21 and 37 GHz channels [Fig. 5(b) and (c)] suggests that the 18-GHz channel drift may completely account for the SSM/I-TMR trend results.

The effect of the 18 GHz channel cold reference brightness temperature drift on the retrieved path delay can be estimated using the approximate global algorithm developed for TMR [8]

$$\begin{aligned} PD(\text{in mm}) &= \text{constant} - 4.8 \cdot \text{TB18} \\ &\quad + 7.3 \cdot \text{TB21} - 0.8 \cdot \text{TB37} \\ \Rightarrow\ \partial(PD)/\partial t &= -4.8 \cdot \partial(\text{TB18})/\partial t \\ &\quad + 7.3 \cdot \partial(\text{TB21})/\partial t - 0.8 \cdot \partial(\text{TB37})/\partial t. \end{aligned} \tag{2}$$

Substituting values of 0.27, 0, and 0 for the TB time derivatives in (2) yields $\partial(PD)/\partial t = -1.3$ mm/yr, equivalent to the result of the SSM/I-TMR global trend comparison and consistent with the other drift assessments shown in Table I.

The source of the 18-GHz channel instrument drift has been tentatively identified as a gradual change in the isolation levels and/or insertion losses between ports of the latching ferrite circulator (cal switch) that switches the source of radiation to the radiometer receivers between the earth-viewing main antenna, the cold space-viewing calibration horns, and the warm load waveguide terminations. The change has been identified by examining raw calibration counts from the cold space-viewing horns, which were recorded on the TMR sensor data record archives. Ideally, the cold space horn counts are sensitive only to the cosmic background brightness temperature of ~2.7 K observed by the calibration horns, together with instrument hardware self-emission, which is corrected for in the antenna temperature calibration algorithm. There is also a small contribution

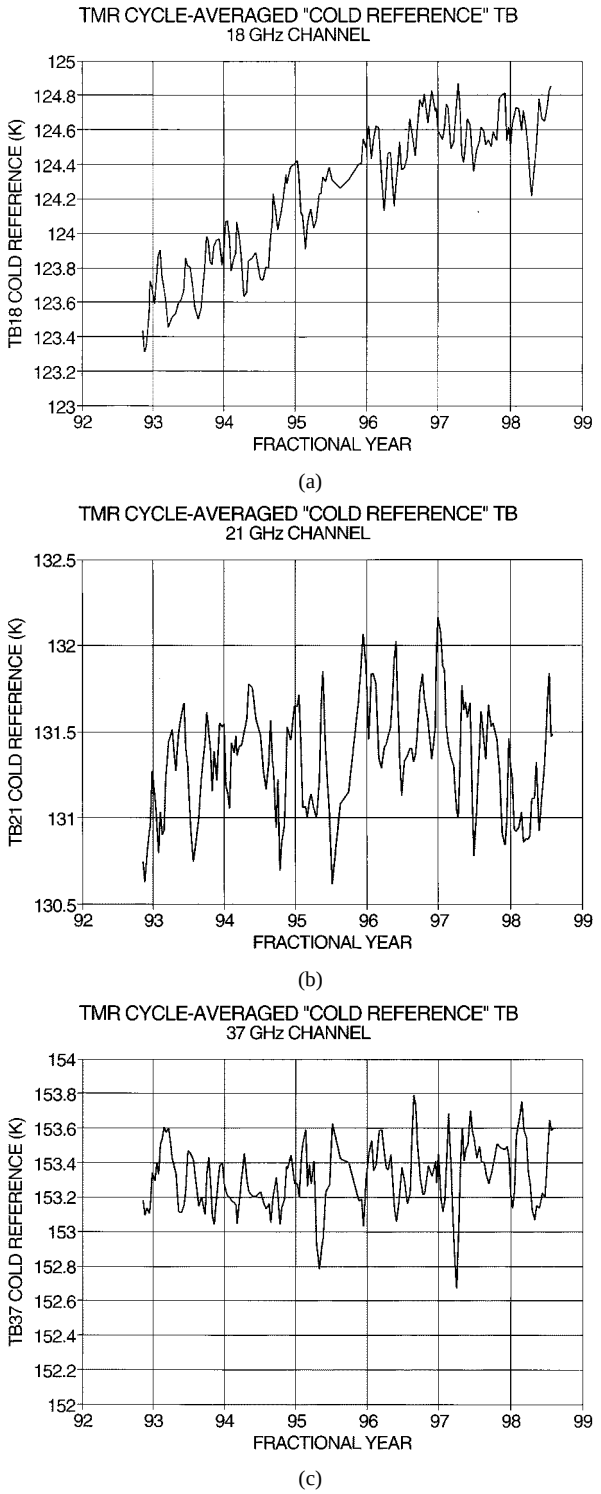

Fig. 5. Cycle-averaged "cold reference" TMR brightness temperatures through mid-1998 (see text). (a) 18-GHz channel, (b) 21-GHz channel, and (c) 37-GHz channel.

to the cold counts from emission by the Earth entering the main antenna due to imperfect isolation in the cal switch. This contribution was determined during preflight thermal/vacuum testing and is also accounted for by the antenna temperature calibration algorithm. The contribution to the cold counts by the earth emission can also be monitored in flight. Cold counts over cold ocean and over warm land brightness temperatures exhibit a systematic difference that corresponds to ~0.5 K when converted using the appropriate radiometer gain relation. This difference is consistent with preflight tests of the cal switch isolation. However, the cycle-averaged land-ocean cold counts were found to have a gradual drift at 18 GHz during 1993–1996, roughly consistent with the 0.27 K/yr drift in the cold reference brightness temperature calibration. During the same period, there was no discernible drift in the land-ocean cold counts at 21 and 37 GHz. In addition, the drift in the land-ocean cold counts at 18 GHz appears to level off in 1997, also consistent with the nature of the cold reference brightness temperature drift. A precise comparison between the identified 0.27 K/yr drift and the drift in calibration that would result from the observed change in the isolation of the cal switch is, however, difficult due to the small size of the leakage signal and to the uncertainty in the radiometer gain equation needed to convert cold counts to equivalent brightness temperatures. The exact cause or causes of the change in cal switch isolation is still under investigation.

V. TMR Scale Error: SSM/I and Radiosonde Comparisons

In addition to the time drift results, the SSMI-TMR and radiosonde-TMR comparisons provide an estimate of the TMR performance in terms of retrieved path delay offsets and scale errors. Errors that vary with the path delay level (scale errors) are particularly troublesome, producing false sea level gradients, especially in the meridional direction, which would be improperly interpreted as meridional sea level slopes and zonal ocean transport. For example, a 5% scale error in the TMR-derived wet delay correction would be erroneously interpreted as a ~2 cm equator-to-pole sea level difference.

The analysis is complicated by the restricted upper and lower limits of atmospheric wet path delay and by the fact that all of the data sets are subject to errors of similar magnitude, including decorrelation errors in the comparisons of measurements separated in time and/or space. The analysis is not compromised by the TMR drift error identified in Section III. Removal of the drift produces no significant change in the scale error results described hereafter, and only a 3–4 mm change in the offset result, far below uncertainty limits due to other error sources.

Consider the scatterplots of radiosonde versus TMR path delay (Fig. 6) and SSMI versus TMR path delay (Fig. 7). Only one representative month of the SSM/I comparison data is shown (out of over 10^6 data points in the 68 months of this study) for clarity. Standard linear regression fits to the radiosonde versus TMR and all of the SSM/I versus TMR path delay data yield

$$PDraob(\text{mm}) = 2.5 + 0.9578 * PDtmr \quad (3a)$$

$$PDssmi(\text{mm}) = 7.6 + 0.9583 * PDtmr \quad (3b)$$

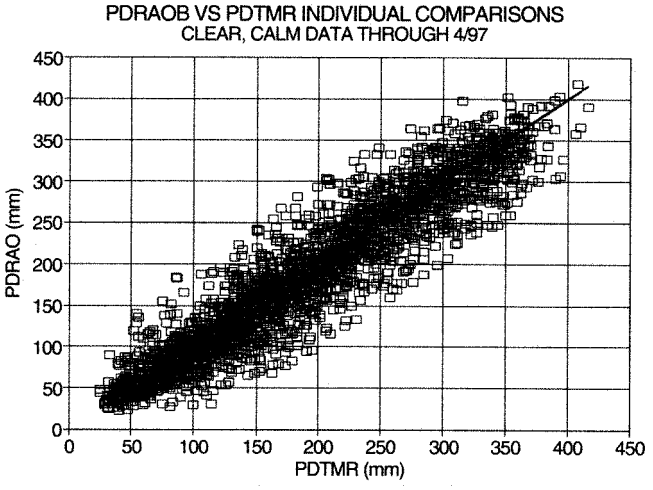

Fig. 6. Scatterplot of radiosonde versus TMR-derived wet path delays for <6 h, 300 km colocation through April 1997.

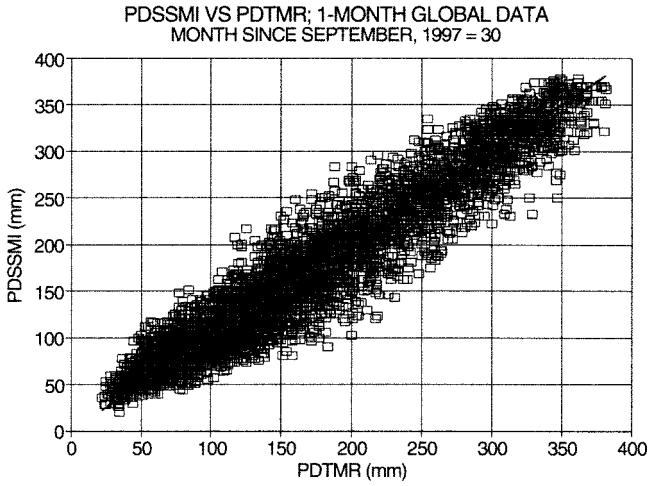

Fig. 7. Scatterplot of SSM/I versus TMR-derived wet path delays for 30-day average, 1° latitude × 1° longitude bins, March, 1995.

which suggests a ~4% scale error in TMR estimates of PD. The problem with this approach is that comparison points at the low and high ends of the path delay distribution skew the determination of scale error due to the finite limits of the measured property.

For example, at the low end, path delay measurements never fall below ~ 20 mm. Thus, for TMR path delay values approaching 20 mm, the radiosonde and SSM/I comparison points are necessarily biased high due to the 20 mm path delay floor. At the high end of TMR path delays, the radiosonde and SSM/I comparison points are biased low due to the scarcity of measured path delay values exceeding 400 mm. If the radiosonde or SSM/I path delays are considered the independent variable, then the opposite conclusion is reached. This characteristic of the comparisons is most clearly illustrated by binning the differences as functions of the measured quantity. For the present cases, the apparent scale error changes sign depending on whether the difference data is binned by TMR path delay level or radiosonde (SSM/I) path delay level.

To properly account for the fact that the two data sets in the scatterplots contain errors (and their finite extent), we use a

modified least squares regression, in which the quantity minimized is the sum of squared distances to the data points measured normal to the regression line, as opposed to the standard approach, in which the vertical separation between data and line is minimized.

When the orthogonal least squares regression is applied to the 10/92–12/96 radiosonde versus TMR and SSM/I versus TMR data sets, the following fits result:

$$PDraob = -8.4 + 1.017 * PDtmr \quad (4a)$$

$$PDssmi = 3.2 + 0.992 * PDtmr. \quad (4b)$$

Within the formal uncertainties of the calculated fits, the slopes derived from the radiosonde versus TMR and SSM/I versus TMR comparisons are not significantly different from unity. The derived offsets are well within the TMR path delay error budget specification (12 mm) and are subject to numerous uncertainties at the 5–10 mm level. Based on these results, we conclude that no significant offset ($>$10 mm) or scale error ($>$2%) is present in the global TMR path delay correction measurements relative to either SSM/I or the island radiosonde reference data.

VI. Summary and Discussion

The performance of the TOPEX microwave radiometer has been evaluated over its first six years of operation using global comparisons with SSM/I and radiosondes in the wet path delay domain. On the global scale, a downward drift in the TMR path delay measurements of 1.3–1.4 mm/yr relative to SSM/I is clearly indicated, beginning at launch and ending $\sim$ December 1996. No significant variation of the drift is seen with either latitude or path delay level. The global drift result is corroborated by our island radiosonde comparison as well as comparisons by other investigators between TMR and GPS [11], the ERS radiometers [10], and the Harvest Platform water vapor radiometer [12]. The derived TMR drift translates directly into a 1.3–1.4 mm/yr artificial decrease in the TOPEX global sea level measurements over the first four years of the mission.

The source of the drift has been quantitatively identified as a hardware drift in the TMR 18-GHz channel, equivalent to $+0.27$ K/yr in measured brightness temperature. The calibration drift was determined by an analysis of the time history of the coldest measured TMR antenna temperatures, a technique that effectively separates instrument-related and atmosphere-related long term trends. The cold reference methodology [20] is generally applicable to water vapor sensing satellite radiometers and is highly recommended for instrument drift monitoring and instrument cross-calibration.

Based on nearly five years of TMR path delay comparisons with island radiosonde and SSM/I data, no significant offset or scale error is seen in the TMR measurements. A modified linear regression was applied to the comparison data, which mitigates the effects of low and high end biases and also partially accounts for temporal and spatial decorrelation errors in the path delay measurements from the two instruments. The modified least squares technique minimizes the sum of the squared orthogonal differences from the best fit line rather than the sum of squared vertical differences. The resulting fits to the SSM/I versus TMR and radiosonde versus TMR data yield apparent TMR scale errors less than 2% and comparable to the statistical error of the slope determinations. Derived offsets are less than 10 mm in magnitude, a level that is subject to numerous uncertainties (e.g. radiosonde measurement errors and the Vz-to-PD conversion of the SSM/I data) in the comparisons with TMR.

It is important to note that the primary data source for in-flight calibration and verification of all satellite radiometer measurements of tropospheric water vapor and path delay is radiosondes. Thus, differences in radiosonde processing, errors in radiosonde humidity measurements (which may vary with the selected radiosonde archive), and differences in the filtering criteria used to eliminate questionable radiosonde data can all contribute to calibration errors at the $\sim$ few percent level of path delay. These uncertainties likely limit our ability to calibrate satellite radiometer measurements of path delay to better than $\sim$3% in scale error and $\sim$10 mm in offset from either direct radiosonde comparisons or comparisons with other satellite instruments.

Acknowledgment

This paper presents the results of one phase of research conducted at the Jet Propulsion Laboratory, California Institute of Technology, Pasadena, under contract with the National Aeronautics and Space Administration, Washington, DC.

References

[1] G. Carlisle, A. DiCicco, H. M. Harris, A. Salama, and M. Vincent, "TOPEX/Poseidon Project Mission Plan," Jet Propulsion Lab., Pasadena, CA, Doc. D-6862, Rev. B, 1991.

[2] L. Fu, E. J. Christensen, C. A. Yamarone, Jr., M. Lefebvre, Y. Menard, M. Dorrer, and P. Esudier, "TOPEX/Poseidon mission overview," *J. Geophys. Res.*, vol. 24, pp. 24 369–24 382, 1994.

[3] C. Le Provost, F. Lyard, J. M. Molines, M. L. Genco, and F. Rabilloud, "A hydrodynamic ocean tide model improved by assimilating satellite altimeter-derived data set," *J. Geophys. Res.*, vol. 103, pp. 5513–5529, 1998.

[4] D. P. Chambers, B. D. Tapley, and R. H. Stewart, "Long-period ocean heat storage rates and basin-scale heat fluxes from TOPEX," *J. Geophys. Res. Oceans*, vol. 102, pp. 10 525–10 533, 1997.

[5] J. F. Minster, A. Cazenave, Y. V. Serafini, F. Mercier, M. C. Gennero, and P. Rogel, "Annual cycle in mean sea level from Topex-Poseidon and ERS-1: Inference on the global hydrological cycle," *J. Global Planet. Change*, vol. 20, pp. 57–66, 1999.

[6] C. Ruf, S. Keihm, and M. Janssen, "TOPEX/Poseidon microwave radiometer (TMR): I. Instrument description and antenna temperature calibration," *IEEE Trans. Geosci. Remote Sensing*, vol. 33, pp. 125–137, Jan. 1995.

[7] M. Janssen, C. Ruf, and S. Keihm, "TOPEX/Poseidon microwave radiometer (TMR): II. Antenna pattern correction and brightness temperature algorithm," *IEEE Trans. Geosci. Remote Sensing*, vol. 33, pp. 138–146, Jan. 1995.

[8] S. Keihm, M. Janssen, and C. Ruf, "TOPEX/Poseidon microwave radiometer (TMR): III. Wet troposphere range correction algorithm and pre-launch error budget," *IEEE Trans. Geosci. Remote Sensing*, vol. 33, pp. 147–161, Jan. 1995.

[9] C. S. Ruf, S. J. Keihm, B. Subramanya, and M. A. Janssen, "TOPEX/POSEIDON microwave radiometer performance and in-flight calibration," *J. Geophys. Res.*, vol. 99, no. C12, pp. 24,915–24 926, 1994.

[10] J. Stum, "A comparison of the brightness temperatures and water vapor path delays measured by the TOPEX, ERS-1, and ERS-2 microwave radiometers," *J. Atmos. Ocean. Technol.*, vol. 15, pp. 987–994, 1998.

[11] B. J. Haines and Y. Bar-Sever, "Monitoring the TOPEX microwave radiometer with GPS: Stability of columnar water vapor measurements," *Geophys. Res. Lett.*, vol. 25, no. 19, pp. 3563–3566, 1998.

[12] D. Kubitschek, G. Born, K. Key, B. Haines, and S. Gill, "Calibration methods for the TOPEX and POSEIDON altimetry systems, (abstract)," *Ann. Geophys.*, vol. 15, p. C196, 1997.
[13] S. Rasool, "Scientific responsibility in global climate change research," *Science*, vol. 283, pp. 940–941, 1999.
[14] R. S. Nerem, B. J. Haines, J. Hendricks, J. F. Minster, G. T. Mitchum, and W. B. White, "Improved determination of global mean sea level variations using TOPEX/POSEIDON altimeter data," *Geophys. Res. Lett.*, vol. 24, no. 11, pp. 1331–1334, 1997.
[15] G. T. Mitchum, "Monitoring the stability of satellite altimeters with tide gauges," *J. Atmos. Ocean. Technol.*, vol. 15, no. 3, pp. 721–730, 1998.
[16] J. P. Hollinger, J. L. Peirce, and G. A. Poe, "SSM/I instrument evaluation," *IEEE Trans. Geosci. Remote Sensing*, vol. 28, pp. 781–790, Sept. 1990.
[17] F. Wentz, "A well-calibrated ocean algorithm for special sensor microwave/imager," *J. Geophys. Res.*, vol. 102, no. C4, pp. 8703–8718, 1997.
[18] F. Wentz and R. W. Spencer, "SM/I rain retrievals within a unified all-weather ocean algorithm," *J. Atmos. Sci.*, vol. 55, pp. 1613–1627, 1998.
[19] G. Boudouris, "On the index of refraction of air, the absorption of dispersion of centimeter waves by gasses," *J. Res. Nat. Bur. Stand., Sect. D*, vol. 67, pp. 631–684, 1963.
[20] C. S. Ruf, "Detection of calibration drifts in spaceborne microwave radiometers using a vicarious cold reference," *IEEE Trans. Geosci. Remote Sensing*, vol. 38, pp. 44–52, Jan. 2000.

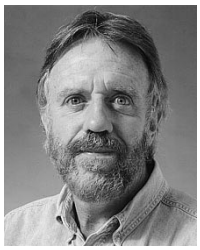

Stephen J. Keihm received the B.S. degree in physics from Fordham University, Bronx, NY, in 1968, the B.S. degree in mechanical engineering from Columbia University, New York, NY, in 1969, and the M.S. degree in astronautical science from Stanford University, Stanford, CA, in 1970.

From 1970 to 1978, he worked as a Research Assistant, then Staff Associate with the Lamont-Doherty Geological Observatory, Columbia University. While at Lamont, he served as Co-investigator for the Apollo 15 and 17 lunar heat flow experiments, and Principal Investigator in studies of the thermal and electrical properties of the lunar regolith. In 1978, he joined the Planetary Science Institute, Pasadena, CA, doing theoretical studies for the interpretation of data from the remote sensing of planetary surfaces. Since 1982, he has worked at the Jet Propulsion Laboratory (JPL), California Institute of Technology, Pasadena. At JPL, he has developed lumar microwave calibration models for the Cosmic Background Explorer (COBE) experiment and worked extensively in the areas of algorithm development and data interpretation for Earth-based aircraft and satellite microwave measurements of the atmosphere and sea surface. His current research activities include design and algorithm development for future satellite microwave instruments and the development of an advanced ground-based water vapor radiometer for tropospheric path delay calibration in the Cassini gravity wave experiment.

Victor Zlotnicki (M'86) studied surveying and geophysical engineering, University of Buenos Aires, Buenos Aires, Argentina, and received the Ph.D. in oceanography from the Massachusetts Institute of Technology, Woods Hole Oceanographic Institution, Woods Hole, MA, in 1983.

He has been with the Jet Propulsion Laboratory, California Institute of Technology, Pasadena, since 1985. His present research interests include applications of altimetry and gravimetry to ocean circulation, accuracy improvements for altimetric data, and the processing and management of large satellite data sets.

Christopher S. Ruf (M'87–SM'92) received the B.A. degree in physics from Reed College, Portland, OR, and the Ph.D. degree in electrical and computer engineering from the University of Massachusetts, Amherst.

He is an Associate Professor of Electrical Engineering at The Pennsylvania State University, University Park, PA, where he has been since 1992. He has worked in semiconductor production engineering for Intel Corporation, and on the Technical Staff, Microwave Observational Systems, NASA's Jet Propulsion Laboratory (JPL), California Institute of Technology, Pasadena. His current research activities include participation in the TOPEX/Poseidon, GEOSAT Follow-On, Jason-1, NPOESS CMIS, and TRMM/GPM flight missions, ground based atmospheric remote sensing using millimeter radars and radiometers, and synthetic aperture interferometric radiometry. He is a past Guest Editor and Associate Editor for *Radio Science*. He serves or has served on the Technical Program Committees of IGARSS '96, '98, '99, and 2000, and of the μRad'96 Specialist Meeting on Microwave Radiometry and is the General Chairman of μRad2001.

Dr. Ruf has received three NASA Certificates of Recognition and three NASA Group Achievement Awards, as well as the 1997 GRS-S Transactions Prize Paper Award and the 1999 IEEE Judith A. Resnik Technical Field Award. He is the current Editor and past Associate Editor of the *IEEE Geoscience and Remote Sensing Newsletter*.